Interseismic strain accumulation along the western boundary of the Indian subcontinent

Walter Szeliga,[1,2] Roger Bilham,[1] Din Mohammad Kakar,[3] and Sarosh H. Lodi[4]

Received 1 September 2011; revised 12 June 2012; accepted 20 June 2012; published 8 August 2012.

[1] Despite an overall sinistral slip rate of ≈3 cm/yr, few major earthquakes have occurred in the past 200 years along the Chaman fault system, the western boundary of the India Plate with the Eurasia Plate. GPS and InSAR data reported here indicate sinistral shear velocities of 8–17 mm/yr across the westernmost branches of the fault system, suggesting that a significant fraction of the plate boundary slip is distributed in the fold and fault belt to the east. At its southernmost on-land segment (≈26°N), near the triple junction between the Arabia, Eurasia, and India Plates, we find the velocity across the Ornach Nal fault is $15.1^{+16.9}_{+13.4}$ mm/yr, with a locking depth probably less than 3 km. At latitude 30°N near the town of Chaman, Pakistan, where a M6.5 earthquake occurred in 1892, the velocity is $8.5^{+10.3}_{+6.8}$ mm/yr and the fault is locked at approximately 3.4 km depth. At latitude 33°N and further north, InSAR data indicate a velocity across the Chaman fault of 16.8 ± 2.7 mm/yr. The width of the plate boundary varies from several km in the south where we observe ≈2 mm/yr of convergence near the westernmost strike-slip faults, to a few hundreds of km in the north where we observe 6–9 mm/yr of convergence, and where the faulting becomes distinctly transpressional. The shallow locking depth along much of the transform system suggests that earthquakes larger than those that have occurred in the historical record would be unexpected, and that the recurrence interval of those earthquakes that have occurred is of the order of one or two centuries, similar in length to the known historical record.

Citation: Szeliga, W., R. Bilham, D. M. Kakar, and S. H. Lodi (2012), Interseismic strain accumulation along the western boundary of the Indian subcontinent, *J. Geophys. Res.*, *117*, B08404, doi:10.1029/2011JB008822.

1. Introduction

[2] The ≈1000-km-long Chaman fault system includes a group of prominent sinistral strike slip fault segments that bound the western edge of the India Plate, and separate it from a southward projecting promontory of the Eurasia Plate to the west [*Wellman*, 1966]. To the east of these sinistral faults, a complex fold and thrust belt verges eastward implying considerable strain partitioning. The width of these fold belts increases from a few tens of km near the Makran coast in the south, to more than 200 km in the north where the fault strikes veer to the NE. Geological and plate closure estimates suggest sinistral slip across the Chaman fault system of between 19 and 35 mm/yr over the last 25 Ma [*Lawrence and Yeats*, 1979].

[3] Three major left-lateral left-stepping faults account for most of the north-south length of the Chaman fault system, the Chaman, Ghazaband, and Ornach-Nal faults (Figure 1). The Chaman fault is the longest of these, extending ≈800 km from 28°N, near the northernmost fold belts of the Makran subduction zone, to 35°N, where the fault branches to the Gardez and Paghman faults to the west and east of Kabul respectively. Despite its considerable length, the only damaging earthquake of note to have occurred on the Chaman fault in the past 200 years (1892, M6.5) occurred near the town of Chaman, Pakistan, to which the fault owes its name [*Griesbach*, 1893]. A major earthquake is inferred to have offset the Paghman fault in 1505 [*Ambraseys and Bilham*, 2003a, 2003b; *Ambraseys and Jackson*, 2003]. To the NE of its intersection with the Herat fault, strike slip motion on the Chaman fault system is transferred to the Kunar Valley fault, the location of a major earthquake in 1842 [*Baird Smith*, 1843; *Ambraseys and Douglas*, 2004].

[4] Between 27°N and 31°N and starting some 40 km east of the town of Chaman, strike slip deformation is increasingly accommodated by the Ghazaband fault. Slip on this fault was responsible for extensive damage to the town of

[1]Cooperative Institute for Research in Environmental Sciences and Department of Geological Sciences, University of Colorado at Boulder, Boulder, Colorado, USA.
[2]Now at Department of Geological Sciences, Central Washington University, Ellensburg, Washington, USA.
[3]Department of Geology, University of Baluchistan, Quetta, Pakistan.
[4]Department of Civil Engineering, NED University of Engineering and Technology, Karachi, Pakistan.

Corresponding author: W. Szeliga, Department of Geological Sciences, Central Washington University, Ellensburg, WA 98926, USA. (walter@geology.cwu.edu)

0148-0227/12/2011JB008822

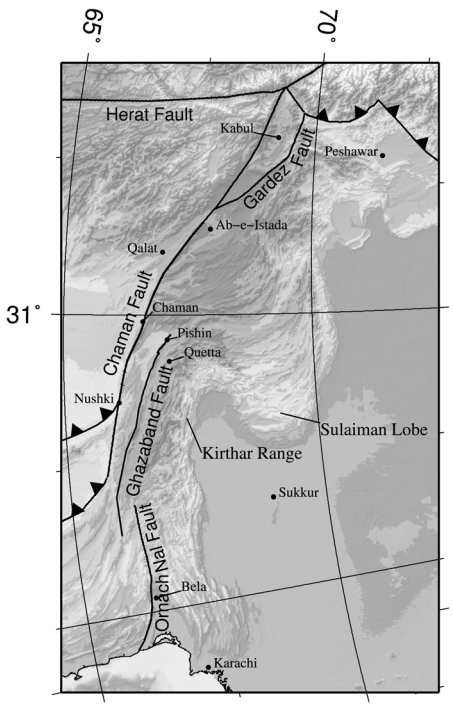

Figure 1. Map of the western boundary of the India Plate highlighting the major faults of the Chaman Fault System; place names mentioned in the text are also indicated. The map projection is oblique Mercator about the pole of relative motion between the India and Eurasia plates. Thrust faults are shown with filled triangles on the hanging wall; all other faults shown are strike slip.

Quetta in an M7.7 earthquake in 1935 [*Cox et al.*, 1936; *Skrine*, 1936; *Ramanathan and Mukherji*, 1938; *Pinhey*, 1938]. Between 25.5°N and 28°N, strike-slip motion is largely accommodated by the ≈250 km long Ornach Nal fault, upon which no major earthquake is known of have occurred in the historical record. The Ornach Nal fault can be traced southwards along the western edge of the Somniani depression toward an offshore triple junction between the Arabia, India and Eurasia Plates.

[5] Few details of earthquakes in the region are available prior to 1800, but it is clear that those major earthquakes that have been observed have ubiquitously ruptured different segments of the plate boundary. Hence, the earthquake cycle along the Chaman fault is far longer than that reliably recorded by the historical record. As a result, we do not know whether significantly large earthquakes than the 1935 Quetta M7.7 may occur along the India plate's western transform system, and we are uncertain of the recurrence interval of those major earthquakes that have occurred. In such circumstances, the geodetic loading rate of the major faults can provide guidance to the tectonic loading rate of each of the faults. However, although several triangulation lines cross the strike-slip faults and the fold and thrust belts that flank them to the east, none have been remeasured since their initial measurements at the turn of the 20th century [*Ambraseys and Bilham*, 2003b].

[6] The measurements presented here thus provide a first glimpse of the loading rate and locking depths of some of the major faults of the Chaman fault system. We analyze data from two campaign GPS transects at 27°N and 30°N and several continuous GPS station on the stable India Plate in Pakistan. Between 31–32°N, we utilize nearly 4.5 years of InSAR data to produce a fault centered transect of interseismic deformation rate. In all three locations we find locking depths to be shallow. The absence of GPS data to the south of Chaman west or east of the Ghazaband fault hinders our ability to estimate interseismic deformation rates across the causal fault of the 1935 Quetta earthquake.

2. Tectonic Summary

[7] The Ornach-Nal fault is the southernmost on-land segment of the Chaman Fault System (Figure 1) [*Zaigham*, 1991; *Lawrence et al.*, 1992]. Running nearly 250 km north from the Makran Coast, the Ornach-Nal Fault offsets primarily Cenozoic mudstones and shales [*Snead*, 1964; *Zaigham*, 1991; *Lawrence et al.*, 1992]. The lack of detailed field mapping in this region, combined with the monotony of the mudstones and shales have made estimates of the total offset across the Ornach-Nal fault impossible.

[8] At the northern terminus of the Ornach-Nal fault, deformation likely steps westward onto the Ghazaband Fault (Figure 1). Although no modern geodetic measurements exists across this segment of the Chaman Fault System, the Ghazaband fault is a likely candidate for the source of the 1935 Quetta earthquake ($\sim M$ 7.5) which caused surface cracking and extensive damage in the populated valleys south of Quetta and approximately 15 km east of the Ghazaband Fault [*Ramanathan and Mukherji*, 1938; *Engdahl and Villasenor*, 2002]. The Ghazaband Fault continues northward to the town of Pishin where it disappears into the southern end of the seismically quiet Katawaz Block [*Haq and Davis*, 1997] (Figure 2a).

[9] South of the village of Nushki, Pakistan, the arcuate thrust faults of the Makran merge to form the N-S trending Chaman Fault (Figure 1). The Chaman Fault and Ghazaband Fault parallel each other northwards to the latitude of the town of Chaman, Pakistan. Immediately north of the town of Chaman, the Chaman fault proper veers NNE, enters Afghanistan and becomes the dominant fault in the Chaman Fault System.

[10] *Lawrence et al.* [1992] estimate the onset of faulting along the Chaman Fault System as Oligocene-Miocene based on post-depositional offsets of the Eocene-Oligocene aged Khojak flysch. These displacements suggest an average slip-rate of 19–24 mm/yr over the last 20–25 My. Similarly, correlation of Pliocene volcanic units that straddle the fault north of Ab-e-Istada, Afghanistan, yields an average slip-rate of 25–35 mm/yr over the last 2 My [*Beun et al.*, 1979].

[11] Kinematic and analogue modeling of the western boundary of the India plate indicates that pure strike-slip motion is required along the Chaman fault with shortening being accommodated in the Sulaiman Lobe and Kirthar ranges to the east of the Chamanfault [*Haq and Davis*, 1997; *Bernard et al.*, 2000]. Estimates of modern plate motion indicate convergence of the India plate relative to Eurasia at a rate of 30 mm/yr at N9E near Sukkur, Pakistan (27.69N, 68.84E) [*Altamimi et al.*, 2011a]. We estimate the amount of sinistral slip along the Chaman Fault by noting that its strike between Chaman and Ab-e-Istada is approximately N34E,

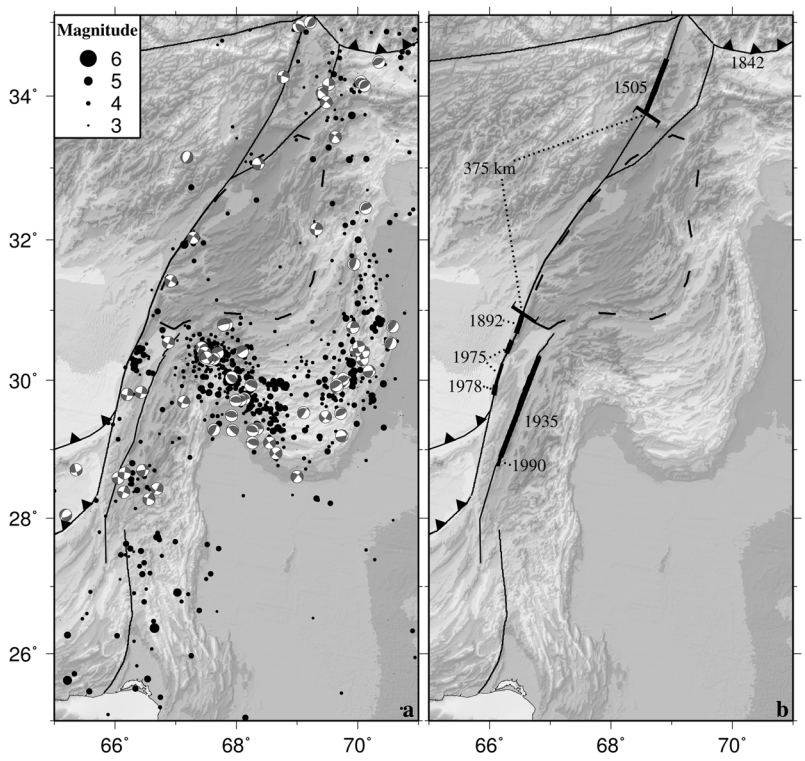

Figure 2. Seismicity and locations of historical fault rupture along the western boundary of the India Plate. The dashed line represents the boundary of the Katawaz Block of *Haq and Davis* [1997]. (a) Earthquake locations from 1964–2010 from the ISC catalog and moment tensors from 1976–2010 from the Global CMT Project. Filled segments of the moment tensors represent the compressional quadrants for the best fitting double-couple. (b) Approximate rupture lengths for major historical strike-slip earthquakes listed in *Wells and Coppersmith* [1994] using published estimates of magnitude. The 375 km segment between the 1892 Chaman earthquake and the 1505 Kabul earthquake has no known major historical seismicity. The 1842 Jalalabad earthquake [*Szeliga et al.*, 2010] was likely a thrust faulting earthquake and is shown for completeness.

suggesting approximately 27 mm/yr of sinistral motion and 13 mm/yr of shortening are being accommodated across the Chaman Fault System.

[12] At least four strike-slip earthquakes with $M > 6$ have been recorded historically on the Chaman Fault (Figure 2b). In 1505, a strike-slip event along the Chaman fault occurred west of Kabul [*Oldham*, 1883; *Babur*, 1912; *Lawrence et al.*, 1992; *Ambraseys and Bilham*, 2003a], in 1892, an M 6.5 strike-slip event occurred near the city of Chaman [*Griesbach*, 1893; *Ambraseys and Bilham*, 2003a], in 1975 an M_S 6.7 occurred mid-way between Chaman and Nushki [*Lawrence and Yeats*, 1979; *Engdahl and Villasenor*, 2002] and in 1978 an M_w 6.1 occurred north of Nushki, Pakistan [*Yeats et al.*, 1979; *Engdahl and Villasenor*, 2002]. Recent seismicity along the fault appears to consist mostly of small, M 3–5, earthquakes primarily located in regions of major historical seismicity (Figure 2a). However, due to the lack of seismic instrumentation in the region, most earthquakes occurring in the Chaman Fault System are poorly located.

[13] Earthquakes along the Chaman Fault appear to consistently rupture to the surface. The 1505 earthquake near Kabul was noted to have surface rupture [*Oldham*, 1883; *Babur*, 1912], while surface rupture from the 1892 Chaman, Pakistan, earthquake offset railroad tracks crossing the fault by 0.75 m [photograph and diagram in] [*Griesbach*, 1893]. Surface rupture along the Chaman Fault from the 1892 earthquake was estimated to extend for at least 60 km with its northernmost mapped extent lying near the town of Chaman, Pakistan [*Griesbach*, 1893; *Landor*, 1902]. Due to its remote location, it is unknown whether the 1975 M_S 6.7 Chaman Fault earthquake between Nushki, Pakistan, and Chaman, Pakistan, produced significant surface rupture. Finally, field investigations by *Yeats et al.* [1979] indicate that the 16 Mar. 1978 M_w 6.1 near Nushki, Pakistan, also ruptured to the surface.

[14] Northward, from the 1892 Chaman rupture to the southern terminus of the 1505 rupture, no major historical earthquakes are noted. A more thorough analysis of this observation using seismic moment release along the Chaman fault system over the last 150 years, led both *Bernard et al.* [2000] and *Ambraseys and Bilham* [2003a] to argue that a significant slip deficit exists along the Chaman fault, particularly north of ~31° latitude.

3. Methods

3.1. Introduction

[15] The relative absence of seismotectonic analyses of the Chaman Fault System compared with other major transform systems around the globe leaves many fundamental

questions unanswered. The harsh landscape and general difficulty of access to the region can make even basic fieldwork problematic. Yet, the ideal natural laboratory afforded by the Chaman Fault System makes it an important location to test hypotheses based on other transform boundaries. This difficulty in accessing the region suggests that research using remote sensing techniques are likely to be most successful.

[16] In this study, we utilize various geodetic measurements to quantify and elucidate tectonic processes along the western boundary of the India Plate. Each of these various measurement techniques provides knowledge of different temporal and spatial aspects of the seismic cycle.

[17] In order to examine patterns in seismicity over the longest temporal span, previous authors have used non-instrumental analysis techniques, mainly archival reports of shaking and destruction caused by large earthquakes [*Ambraseys and Bilham*, 2003a, 2003b; *Szeliga et al.*, 2010]. With certain caveats, these macroseismic data may be analyzed to provide coarse resolution of epicentral location and magnitude and thus act as a rough estimate for regional strain rates.

[18] Geodetic data in the form of direct surface height measurements and horizontal distances may be obtained using spirit-leveling and triangulation. These data, first collected on the Indian subcontinent during the late 19th century [*Ambraseys and Bilham*, 2003b], provide constraints on geoid height and baseline length along a transect, and, when combined with prior observations, differential positions. The effort involved in collecting both triangulation and spirit-leveling data with a high temporal resolution results in infrequent reoccupation of benchmarks with detailed spatial coverage over limited areas (typically <1 km transects). Unfortunately, triangulation networks that cross the Chaman Fault System have never been remeasured [*Ambraseys and Bilham*, 2003b]. Modern estimates of height are routinely measured along with high precision location estimates using GPS receivers. When continuously operated from a permanent stable benchmark, relative positions may be obtained to an accuracy of 2–5 mm horizontally and 6–15 mm in height [*Segall and Davis*, 1997]. While continuously operating GPS stations provide a vast improvement over spirit-leveling and triangulation in the temporal domain, they suffer in the spatial domain in being essentially point measurements and are often separated by large distances (20–200 km). Synthetic Aperture Radar (SAR) data provide dense spatial coverage at the expense of temporal resolution for geodetic applications. Interferometric SAR (InSAR), produced by differencing two SAR scenes, provides information about the relative motion of the ground when the SAR scenes are obtained at different times from similar vantage points. Deformation data obtained by any single InSAR image provides spatially dense measurements of only one component of deformation, and can limit the capability of using InSAR alone to fully describe a deformation field [*Bürgmann et al.*, 2000]. However, this high spatial density of deformation information at low temporal sampling complements GPS positioning data. Although it is possible to translate measured phase differences from an InSAR image to mm precision line-of-sight measurements, the relationship between phase measurement and ground deformation is dependent on the atmospheric conditions along the line-of-sight during the acquisition of each SAR scene [*Massonnet and Feigl*, 1995]. These caveats require the use of multiple InSAR scenes to help discriminate between ground deformation and atmospheric signals. In general, fault azimuths in Chaman Fault System south of Chaman, Pakistan, are incompatible with the orbits of current SAR satellites, providing little or no deformation-resolving power in their along strike direction. However, the change in fault strike north of Chaman, Pakistan, combined with the arid climate and general lack of vegetation in the region makes this location desirable for study using InSAR.

3.2. GPS

[19] GPS measurements in Pakistan are historically of limited coverage and duration with no known measurements prior to 2001. Campaign measurements from 7 sites with locations predominantly north of Quetta as well as 5 sites in southern Baluchistan province, have been measured at least twice in the period 2006–2012 and compared to continuous measurements made at 23 IGS regional station, plus stations in Karachi (KCHI), Sukkur (SIBA), and Quetta (QTAG and QTIT) (Figure 3 and Table 1).

[20] The location of campaign GPS measurements across both the Chaman and Ornach-Nal faults are constrained by the location of major roads to provide security and ease of access. The continuous points in Pakistan are operated from flat-roofed concrete frame buildings and the campaign points are measured on bipods set on stainless steel screws cemented into exposed bedrock. GPS observations were recorded with Trimble NetRS, 5700 and R7 receivers using a 30 s sampling rate, and processed using an elevation cutoff angle of 10°. Campaign data have durations of 3–7 days per occupation from each site.

[21] Our GPS data analysis methodology is as follows, first, we use daily GPS phase observations to estimate station position and atmospheric delay while holding IGS final orbits fixed to produce loosely constrained estimates of station positions and covariances using GAMIT version 10.40 [*Herring et al.*, 2010a]. These loosely constrained estimates of station positions and covariances are then used as input to GLOBK version 5.19 [*Herring et al.*, 2010b] to estimate a consistent set of station coordinates and velocities. We tie our regional measurements to an external global reference frame by simultaneously processing phase data from 23 IGS stations, evenly distributed in azimuth relative to our network.

[22] To account for correlated noise in our measurements, we estimate parameters for a first-order Gauss Markov process noise from each time series using the "real sigma" method [*Herring*, 2003; *Reilinger et al.*, 2006]. These first-order Gauss-Markov parameters can then be used to formulate an equivalent random walk process noise model to be used in a final run of the GLOBK Kalman filter. This final GLOBK run produces a station velocity solution with realistic uncertainty estimates.

[23] Comparison of the uncertainty estimates from GLOBK using the above procedures with the results of analysis of select time series using CATS [*Williams*, 2008] yields similar results.

[24] We realize the ITRF2008 reference frame by minimizing the difference between the positions and velocities

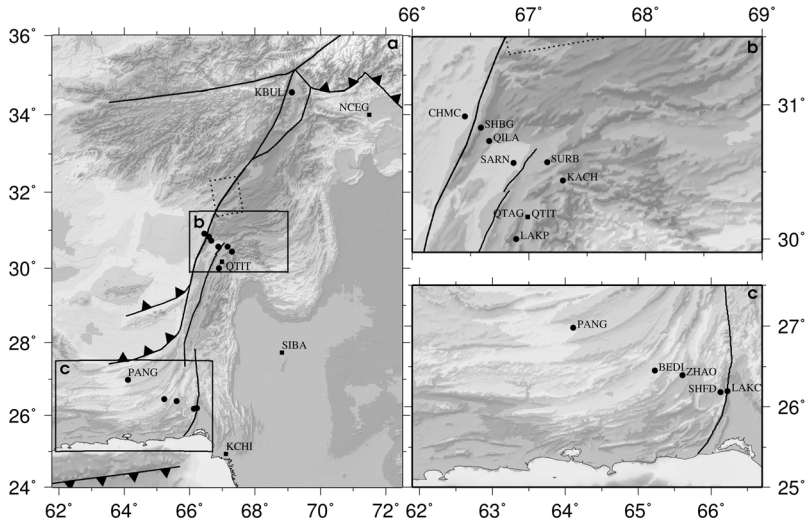

Figure 3. Map showing GPS station locations and names along the western boundary of the India Plate. Continuous GPS stations are indicated by a square, campaign GPS stations are shown as circles. (a) GPS stations throughout Pakistan. Dashed rectangle indicates the ground footprint of Envisat track 213 frame 621. (b) Stations in the Quetta Syntaxis where there is a high station density. (c) Stations along the Makran Coast.

of our 23 processed IGS stations with those published in *Altamimi et al.* [2011b], resulting in a post-fit RMS of 1.29 mm in position and 0.54 mm/yr in velocity. We then rotate our station velocities into an India plate fixed reference frame using the pole-of-rotation parameters published in *Altamimi et al.* [2011a].

3.3. InSAR

[25] We acquired 27 ascending pass SAR scenes spanning nearly 4.5 years from track 213 frame 621 of the European Space Agency's Envisat satellite (Figures 3a and 4). A 90 meter resolution DEM was constructed from SRTM version 2 data [*Farr et al.*, 2007] and used to remove topographic fringes. Interferograms were produced using the ROI_PAC InSAR software package developed at the Jet Propulsion Laboratory in Pasadena, CA [*Rosen et al.*, 2004]. Interferograms were sampled with 8 looks in range and 40 looks in azimuth to produce 160 m × 160 m resolution cells, filtered using a power spectral method [*Goldstein and Werner*, 1998] and unwrapped using a least squares methodology [*Goldstein et al.*, 1988].

[26] Scene selection was guided by visual inspection of interferograms and application of pair-wise logic [*Massonnet and Feigl*, 1995]. From the set of 27 ascending pass scenes, we select 12 SAR image pairs that minimize both temporal and spatial baselines while avoiding scenes that are visually impacted by atmospheric noise (Figure 4). These 12 scenes are then used to form a rate-map using the iterative methodology

Table 1. GPS Velocities Relative to the Stable India Plate as Defined by *Altamimi et al.* [2011a][a]

Site	Longitude	Latitude	Occupations	Time Span	E Velocity (mm yr^{-1})	E Sigma (mm yr^{-1})	N Velocity (mm yr^{-1})	N Sigma (mm yr^{-1})	Rho
PANG	64.11	26.98	2	2008.4–2010.1	−3.5	0.8	−23.8	0.7	0.039
BEDI	65.23	26.45	2	2008.6–2010.0	−0.6	1.3	−14.2	1.2	−0.054
ZHAO	65.61	26.39	2	2008.5–2010.0	0.2	0.8	−13.2	0.8	0.027
LAKC	66.22	26.20	3	2006.0–2008.3	−0.7	0.5	1.5	0.5	0.012
CHMC	66.45	30.91	4	2007.1–2012.2	−3.1	0.3	−20.8	0.2	0.007
SHBG	66.59	30.83	3	2007.1–2008.8	0.5	0.9	−15.4	0.9	−0.015
SHFD	66.13	26.18	2	2008.4–2009.6	0.3	0.8	−1.9	0.7	0.017
QILA	66.66	30.73	4	2007.1–2012.2	−1.8	0.3	−15.3	0.3	0.021
LAKP	66.89	30.00	3	2008.6–2009.7	−4.9	3.2	−12.7	2.7	−0.022
SARN	66.87	30.57	6	2007.1–2012.2	−3.6	0.3	−13.6	0.3	0.007
QTIT	66.99	30.16	c	2008.6–2012.2	−11.1	0.3	−19.0	0.2	0.002
QTAG	66.99	30.17	c	2006.5–2008.7	−5.8	1.1	−7.7	0.3	0.001
SURB	67.16	30.57	5	2007.1–2011.0	−12.7	0.4	−11.3	0.3	0.023
KCHI	67.11	24.93	c	2006.0–2012.2	−1.4	0.1	1.2	0.1	−0.001
KACH	67.29	30.44	5	2007.1–2012.2	−1.1	0.5	−7.9	0.5	0.044
SURB	67.16	30.57	5	2007.1–2011.0	−6.5	0.5	−12.6	0.5	0.036
SIBA	68.82	27.73	c	2008.4–2012.2	−1.8	0.1	1.2	0.1	0.001
KBUL	69.13	34.57	2	2006.2–2008.2	0.9	0.3	−20.6	0.4	0.034
NCEG	71.49	34.00	c	2001.2–2012.2	−1.5	0.1	−3.4	0.3	0.000

[a]Continuous GPS stations are denoted by a "c" in the occupations column.

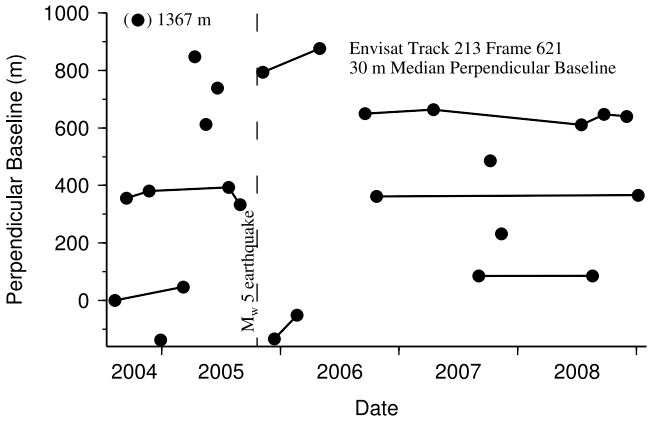

Figure 4. Date versus perpendicular baseline plot for Envisat track 213, frame 621. Filled circles represent individual SAR scenes and solid lines represent interferograms. There is one perpendicular baseline outlier indicated on the correct date in parenthesis along side the associated perpendicular baseline value. The vertical dashed line corresponds to an M_w 5.0 earthquake on 21 Oct. 2005 along the Chaman fault in the northern portion of Envisat track 213 frame 621. The 12 interferograms shown have a median perpendicular baseline of 30 m, corresponding to an altitude of ambiguity of more than 450 m.

outlined in *Biggs et al.* [2007]. Formation of the rate-map utilizes a pixel-based weighted least squares approach with a variance-covariance matrix that accounts for estimates of atmospheric phase delay and orbital uncertainty from each interferogram.

[27] To estimate variance-covariance parameters for errors due to atmospheric phase delay, we analyze a 48 × 48 km region from the tectonically quiet, southeastern corner of each interferogram. We determine a best fit 1-D covariance function of the form

$$c(r) = \sigma^2_{atm} e^{(-\alpha r)}, \tag{1}$$

where σ^2_{atm} is the variance, r is the distance between pixels and α is the e-folding length. Parameters in equation (1) are estimated from the radially averaged 2-D autocovariance function calculated using the cosine Fourier transform of the power spectrum [*Hanssen*, 2001; *Parsons et al.*, 2006]. The estimated atmospheric variance (σ^2_{atm}) and e-folding length (α) are then used to weight pixels in each interferogram during formation of the rate-map.

[28] Although we use ROI_PAC to remove the effects of baseline separation by approximating the earth as a smooth ellipsoid, imperfect knowledge of the satellite's orbit occasionally results in apparent deformation in the form of a residual tilt spanning the InSAR scene. Since the interseismic deformation signal sought is inherently long-wavelength, estimating the residual orbital correction by simply removing a best fitting plane of the form

$$z = ux + vy + w, \tag{2}$$

where x and y are, respectively, the across-track and along-track directions in radar coordinates and u, v and w are the unknowns to be estimated, would result in the removal of a portion of the tectonic signal. To minimize this effect, we estimate orbital corrections using equation (2) from regions as far from the expected deformation signal as possible by masking out a swath 50 km wide, centered on the fault. We then calculate variance-covariance parameters for uncertainty in the orbital correction using the standard deviation of the parameters estimated in equation (2). Residual orbital parameters for our 12 scenes are consistent with results in *Biggs et al.* [2007] of between 0.5 and 1.5 fringes per frame.

4. Results

4.1. Ornach-Nal

[29] We project the GPS velocity field of stations spanning the Ornach-Nal Fault into fault normal and fault perpendicular directions based on the azimuth of the surface trace of faulting west of Bela (~1°, Figures 5 and 6). Two GPS stations (LAKC and SHFD, see Figure 3) straddle the subaerially exposed mud ridges that comprise what appears to be the active trace of the Ornach-Nal Fault. However, Figure 6 shows that the majority of the sinistral motion across the plate boundary occurs west of this mud ridge, between stations SHFD and ZHAO (Figure 3c).

[30] Assuming that interseismic deformation across the plate boundary is accommodated by a single fault with an unknown location, Markov-Chain Monte-Carlo analysis [*Mosegaard and Tarantola*, 1995] of the velocity profile indicates that the data are most consistent with an interseismic deformation rate of 15.1 mm/yr with a 95% Baysian High Posterior Density (95% HPD) region of 13.4–16.9 mm/yr and a locking depth of 2.9 km with a wide 95% HPD of 0 km to 9.1 km. Similarly, estimation of the fault location suggests that the plate boundary lies approximately $12.5^{+35}_{+5.6}$ km west of the mud ridge originally thought to represent the plate boundary (Figure 7). This fault location is associated with a 95% HPD region spanning nearly 30 km, indicating a large uncertainty. The majority of these locations lie beneath the large Hingjal synform and are

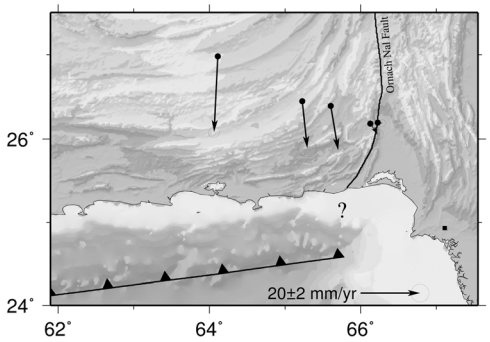

Figure 5. GPS velocities of stations from the Makran region of Pakistan. All velocities are relative to the stable India Plate as defined in *Altamimi et al.* [2011a] and are plotted using a Mercator projection. The exact location of the offshore intersection of the subduction zone and the Chaman fault system is unknown and is denoted with a question mark. Station names appear on Figure 3c.

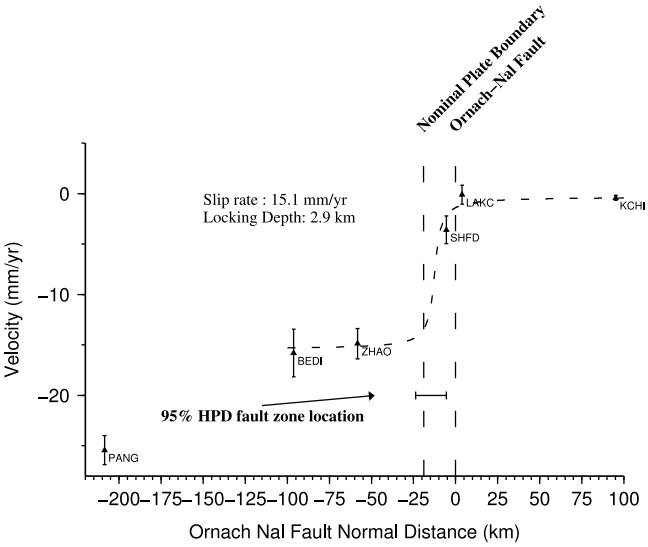

Figure 6. GPS profile across the Ornach-Nal Fault. Velocities and uncertainties are projected into a direction parallel to the Ornach-Nal Fault and are relative to the stable India Plate. Uncertainties shown are 2σ. The thick horizontal bar indicates the 95% HPD range for possible fault locations. The dotted line represents the model that maximizes the empirical posterior likelihood function as determined using a Markov-Chain Monte Carlo method [*Mosegaard and Tarantola*, 1995]. The slip rate and locking depth for the fault location that satisfies both the posterior likelihood and geological criteria (the nominal plate boundary) are indicated on the figure.

consistent with lineations extending north and south of the synform (Figure 7).

[31] Previous authors have suggested that the mud ridges west of Bela are eruptive features [*Jones*, 1961; *Bannert et al.*, 1992]. However, reanalysis of outcrop lithology by *Delisle et al.* [2002] as part of a systematic study on mud volcanism in Pakistan indicates that the mud ridge (Figure 7) is actually an outcrop of Parkini mudstone exposed in the core of an anticline, in stratigraphic sequence, and not part of an eruptive feature. The Parkini mudstone is the source material for mud erupted from mud volcanoes farther south and west of Bela.

[32] The velocity of the site at Panjgur, Pakistan (PANG), is nearly 82% of the expected ITRF2008 rate [*Altamimi et al.*, 2011a]. This observation combined with the low velocities of both SHFD and LAKC relative to the stable India Plate suggests that the remaining plate boundary deformation occurs across faults on the Eurasian side of the plate boundary. It is also notable that the Ornach-Nal parallel velocity of the site in Panjgur (PANG, Figures 3 and 6) is 10.0 ± 0.72 mm/yr faster than the expected far-field velocity due solely to slip on the Ornach-Nal fault. This disagreement is likely due to unmodeled convergence along the arcuate faults that comprise the subaerial Makran forearc between Bedi and Panjgur, Pakistan (GPS stations BEDI and PANG).

[33] The resolved fault normal motion in Figure 5 shows convergence along the line of the section at <2 mm/yr. The subsurface strike of the active Ornach-Nal Fault, however, is not resolved by our sparse geodetic data. Assuming the fault consists of a pair of NNE trending, left-stepping en-echelon sinistral faults, as suggested by surface morphology, and the local synthetic slip vector of the India plate as defined by the ITRF2008 velocity field [*Altamimi et al.*, 2011a] would result in fault normal convergence of ~10 mm/yr.

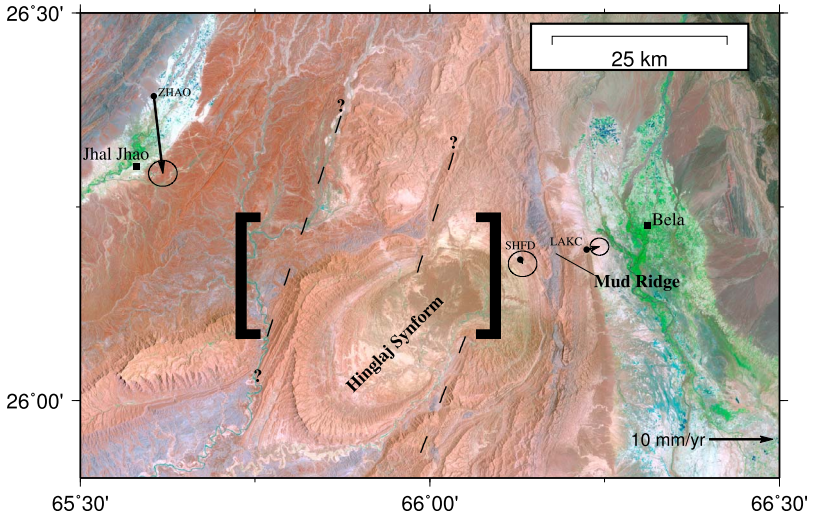

Figure 7. Landsat 7 image of the southern Ornach Nal fault and adjacent Hinglaj synform. The large square brackets indicate the spatial region encompassed by the 95% HPD region shown in Figure 6. NNE trending dashed lines follow surface lineations aligned with surface morphology and mud volcanoes. The region between the fault tips corresponds to the deepest part of the synform [*Bannert et al.*, 1992] consistent with a sinistral pull apart structure. GPS velocities are relative to the stable India Plate and are identical to those shown in Figure 5. The image is a combination of bands 7, 4 and 2 to highlight geological information.

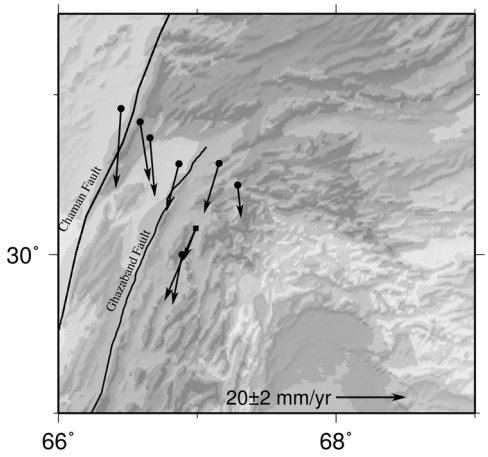

Figure 8. GPS velocities of stations in the region of Quetta, Pakistan. All velocities are relative to the stable India Plate as defined in *Altamimi et al.* [2011a] and are plotted using a Mercator projection. Station names appear on Figure 3b.

4.2. Chaman Fault Near Chaman

[34] We project the GPS velocity field of stations north of Quetta, Pakistan, onto a Chaman Fault perpendicular profile (108.5°) and calculate both fault-parallel and fault-normal velocities (Figures 8 and 9). The location of the profile at this latitude samples the surface deformation field near the intersection of the east-verging folds of the Kirthar Range and the SE verging folds of the Sulaiman Lobe, close to the 20 degree restraining bend in the Chaman Fault, complicating the velocity field. On Figure 9, a step in the velocity profile, consistent with sinistral motion, is evident between stations CHMC and SHBG, which we interpret to be the result of aseismic shear at depth beneath the Chaman Fault at a rate of 8.5 mm/yr (95% HPD range of 6.8–10.3 mm/yr) with a shallow locking depth (3.4 km with a 95% HPD range of 0–7.0 km). Further, the geodetic data may be interpreted to be consistent surface creep on the Chaman Fault, although it has not been reported from field observations.

[35] Although located only 8 km from the trace of the Chaman Fault, station CHMC is moving at approximately 75% of the expected ITRF2008 velocity [*Altamimi et al.*, 2011a]. This observation suggests that most of the plate boundary motion is accommodated by faults on the India Plate east of the Chaman Fault. This is in contrast to observations in the Ornach-Nal region (section 4.1) where diffuse deformation appears to be accommodated primarily on the Eurasia Plate. Further, the location of Sukkur (SIBA) on the stable India Plate combined with the velocity profile in Figure 9 indicates that the remaining 12 mm/yr of sinistral motion must be accommodated across structures east of the Chaman Fault.

[36] Convergence in the Kirthar range is 6.8 ± 1.0 mm/yr, as calculated using a weighted mean of the following stations CHMC, SHBG, QILA. Station SARN appears to display a large seasonal signal in its east component yielding a convergence estimate of 0 mm/yr. Since SARN is a campaign GPS site, the temporal spacing of occupations disallows any meaningful estimates of any periodic signal and thus has been disregarded. The nearly uniform convergence signal observed at the remaining stations west of Quetta suggests that shortening in the Kirthar Range is focused along structures east of Quetta, such as the Dezghat-Bannh Fault System which ruptured during the 1931 Mach earthquake [*Szeliga et al.*, 2009].

4.3. Chaman Fault Near Qalat

[37] North of Chaman, Pakistan, the Chaman Fault enters a 20 degree restraining bend and the fault trend becomes more perpendicular to the azimuth of ascending Envisat satellite passes (approximately 346°). This favorable geometry increases the amount of fault parallel motion visible in the radar line-of-sight compared with locations further south along the Chaman Fault. Descending satellite passes were avoided as the azimuth of such passes relative to the fault strike makes any strike-slip motion geometrically invisible. We have produced a best fitting rate map using 12 Envisat scenes (Figure 10) and calculated line-of-sight displacements through binning of observations by distance from the fault trace. Estimates of line-of-sight displacement for each bin are then calculated using a least squares approach (Figure 11).

[38] In Figure 11, slip-rate and fault-locking-depth are estimated using the two-dimensional strike-slip model of *Savage and Burford* [1973], and uncertainties in rate and depth are determined using a Monte Carlo resampling technique [*Wright et al.*, 2001]. The slip-rate and locking depth estimates of 1.91 ± 0.31 rad/yr in the radar line-of-sight are consistent with 16.8 ± 2.7 mm/yr of fault parallel motion beneath a locking depth of 5.4 ± 2.4 km.

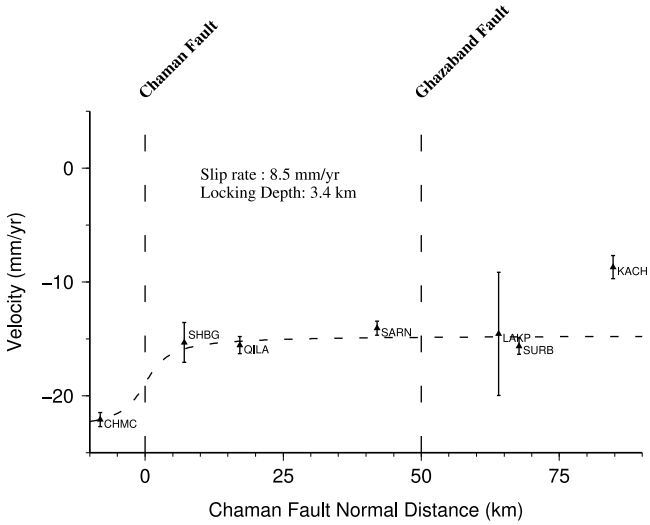

Figure 9. GPS profile across the Chaman Fault. Velocities and uncertainties are projected into a direction parallel to the Chaman Fault and are relative to the stable India Plate. Uncertainties shown are 2σ. The dotted line represents the model that maximizes the empirical posterior likelihood function as determined using a Markov-Chain Monte Carlo method [*Mosegaard and Tarantola*, 1995]. The slip rate and locking depth for this model are indicated on the figure.

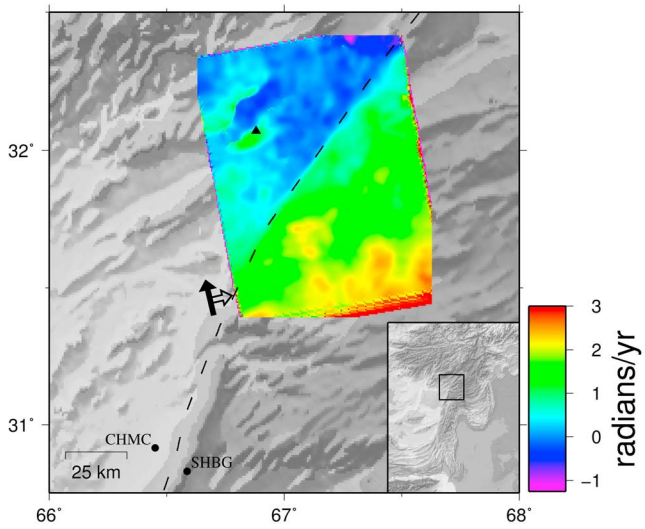

Figure 10. InSAR rate-map derived from stacking 12 ascending pass Envisat interferograms. Solid arrow indicates the flight direction of the satellite while the transparent arrow indicated the line-of-sight direction. Values are phase velocity in rad/yr in the line-of-sight of the radar and referenced to a pixel in the far NW corner of the scene. More positive values of phase velocity indicate increasing radar line-of-sight distance. Interferograms used in construction of the rate-map are indicated by solid lines in Figure 4 and have a median perpendicular baseline of 30 m. The surface trace of the Chaman Fault is indicated by the dashed line. For reference, the locations of GPS stations CHMC and SHBG are indicated in the southern portion of the map. The increasing radar line-of-sight velocities near the town of Qalat, Afghanistan, (black triangle) are likely tied to subsidence due to groundwater withdrawal for agriculture.

[39] A prominent feature seen in both the best fit rate-map and the fault-centered profile is the deformation in the Tarnak Rud valley near the village of Qalat. Analysis of the deformation around the Qalat area using a short-baseline methodology shows nearly 15 mm/yr of deformation in the line-of-sight of the radar during the time period 10 Aug. 2004–6 Jan. 2009 (Figure 12) [*Berardino et al.*, 2002; *Hooper*, 2008]. Comparisons between Landsat 7 band combination 4,3,2 and the InSAR data show a good correspondence between areas of subsidence and modern river channels. The region of greatest subsidence is located downstream of the region of densest agricultural usage but close to the region of densest population (Figure 12b), suggesting that the most probable cause of the deformation is groundwater withdrawal. As Landsat 7 data acquired after 31 May 2003 contains data gaps due to an instrument failure, only data prior to the short-baseline time period are available. It is possible that in the time between when the Landsat 7 shown in Figure 12 was acquired and 6 Jan. 2009, that agricultural land-use in the region surrounding the deformation signal changed.

5. Gardez Fault Near Kabul

[40] North of Ab-e-Istada, the Chaman fault system bifurcates, with the Chaman fault proper continuing north and west of Kabul and the Gardez fault continuing north and east of Kabul [*Lawrence et al.*, 1992] (Figure 1). This region is characterized by mountainous terrain, primitive roads and has relatively few GPS sites. We utilize two GPS measurements, one continuous station located in Peshawar, Pakistan (NCEG) and one campaign GPS station in Kabul, Afghanistan (KBUL) to estimate the total strike-slip and convergence rate across this remote region of the Chaman fault system (Table 1). Although Kabul, Afghanistan is located

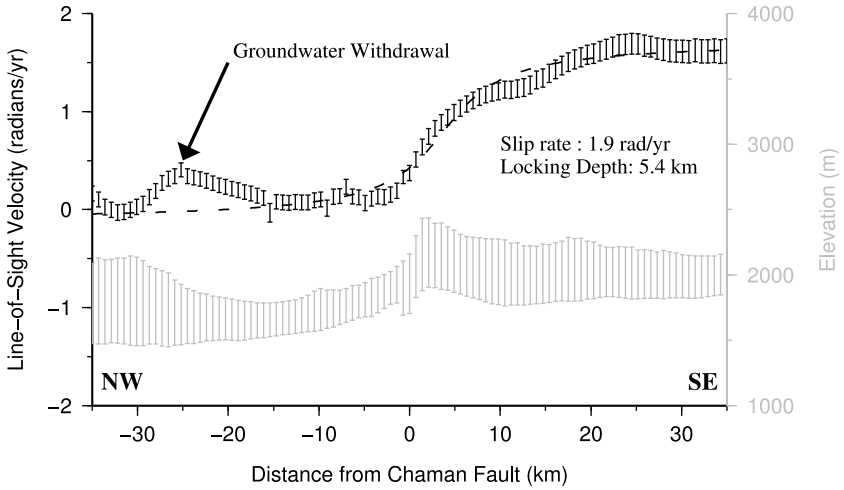

Figure 11. Chaman fault centered profile of line-of-sight velocities from the InSAR rate-map shown in Figure 10. Increasing line-of-sight velocities represent motion away from the radar. The gray data are SRTM level 2 3s topography sampled in the same manner as the InSAR data. Larger variances in the topographic data indicate larger changes in topography parallel to the Chaman fault. The dashed line corresponds to the Monte Carlo derived model. Slip rate and locking depth are calculated in the radar line-of-sight. The convex-up feature 25 km northwest of the Chaman Fault corresponds with groundwater withdrawal near the town of Qalat, Afghanistan.

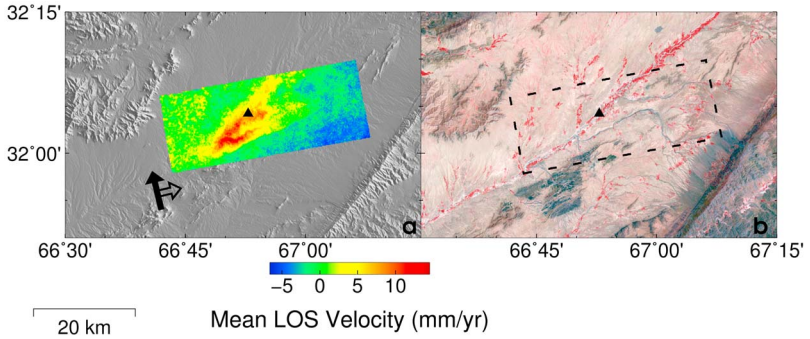

Figure 12. Comparison of InSAR short-baseline results and Landsat 7 imagery from the Tarnak Rud valley near the town of Qalat, Afghanistan. (a) Line-of-sight (LOS) rate map of ground subsidence near the town of Qalat, Afghanistan (triangle). Positive values indicate motion away from the radar. Solid arrow indicates the flight direction of the satellite and outlined arrow denotes the line-of-sight direction of the satellite. Black triangle marks the location of the town of Qalat and is the same as in Figure 10. (b) Landsat 7 image from 18 May 2003 using band combination 4,3,2 to highlight vegetation (red areas).

between the two most prominant strike-slip faults in the northern Chaman fault system, the Chaman fault proper and the Gardez fault, the observed velocity of GPS station KBUL is 76% of the rate expected for stable Eurasia from ITRF2008 [*Altamimi et al.*, 2011a]. Further, while our GPS station locations are not optimally located to precisely identify the active faults in the Chaman fault system at this latitude, we may assume that all of the strike-slip motion is accommodated on faults with the same orientation as the Chaman and Gardez fault at this latitude (~22.5°). Decomposing the baseline velocity between GPS stations in Peshawar, Pakistan (NCEG) and Kabul, Afghanistan (KBUL), we observe a total of 16.8 ± 0.51 mm/yr of sinistral motion and 9.2 ± 0.39 mm/yr of convergence.

6. Discussion

[41] Great earthquakes in the past millennium form an almost continuous line of ruptures along India's northern and eastern boundaries with Eurasia. In contrast, few reports of major earthquakes exist for the Chaman fault system, the two largest on record being the Quetta earthquake of 1935 (M_w 7.7) and, from its reports of widespread damage to cities and ground disruption, the 1505 earthquake reported in the diaries of Babur [*Babur*, 1912; *Ambraseys and Bilham*, 2003a]. The rupture lengths of these two earthquakes currently remain unquantified, but it is possible that each earthquake ruptured upwards of 300 km of the 1200 km long Chaman system, thereby leaving slip on the remaining 600 km to be accounted for in undocumented historical earthquakes, or by processes of aseismic slip (Figure 2b).

[42] The geodetic measurements presented here provide both a measure of the slip rate on the principal faults of the Chaman system, and a clue as to the probable absence of a record of great earthquakes. From continental scale geodesy we know that India's relative velocity with respect to Eurasia at the longitude of the Chaman fault system is 24–28 mm/yr. Our measurements across the Chaman fault reveal that $15.1^{+16.9}_{+13.4}$ mm/yr of this slip is accommodated by the Ornach Nal fault and the central and southern Chaman fault.

[43] Our measurements are unfavorably disposed to quantify the slip rate on the central Ghazabad fault segment, however near the town of Chaman, Pakistan (30.89°N, 66.51°E), we observe an interseismic deformation rate of $8.5^{+10.3}_{+6.8}$ mm/yr across the Chaman Fault, with a total of 22.1 ± 0.3 mm/yr of sinistral motion accommodated between Chaman and Sukkur, Pakistan. The Ghazaband Fault, according to recently relocated epicenters published by *Engdahl and Villasenor* [2002] is likely to have hosted the 1935 Quetta earthquake. Our GPS transect crosses the Ghazaband Fault at its northern extremity near the town of Pishin, and fails to reveal any significant localized shear across it.

[44] Our measurements are unfavorably disposed to quantify the slip rate on the central Ghazaband fault segment, however, near the town of Chaman, Pakistan (30.89°N, 66.51°E), we observe an interseismic deformation rate of $8.5^{+10.3}_{+6.8}$ mm/yr across the Chaman fault, which is presumably the loading rate applicable to a recurrence of the 1892 earthquake. Slip in the 1892 earthquake was measured in only one location as 75–80 cm which would suggest a renewal time for earthquake recurrence of 100 years, with large uncertainty.

[45] The low rate observed at Chaman, Pakistan, leaves a total of 22.1 ± 0.3 mm/yr of sinistral motion unaccounted for between Chaman, Pakistan and Sukkur, Pakistan, which effectively lies on the rigid India Plate to the east of the Seistan ranges. Whether or not the 22 mm/yr of shear displacement is entirely accommodated by slip on the Ghazaband fault is unclear, and although no alternative major fault exists at this latitude, we cannot exclude the possibility of block rotation or distributed shear in the Seistan Ranges to the east. Our GPS transect crosses the Ghazaband fault at its northern extremity near the town of Pishin, Pakistan, and fails to reveal any significant localized shear across it. Slip in the 1935 Quetta, Pakistan earthquake was not measured directly, but scaling laws and seismic moment calculations suggest that with an M7.7 with inferred rupture dimensions of 300 × 12 km it may have slipped 3–5 m which would suggest a renewal time of 150–250 years. No previous earthquakes however, are known in the historical record with this magnitude.

[46] In contrast to the locking depth inferred for the Ghazaband fault, we find significant evidence that shallow locking depths prevail along both segments of the fault where we have examined the velocity field in detail. The Ornach Nal fault, and the southern and central Chaman faults are apparently locked only in their uppermost 3 km, reducing the accumulation of a significant seismic moment deficit. These segments of the fault thus resemble the creeping and transition parts of the San Andreas and Hayward faults, with the exception that no surface creep has been reported from Baluchistan and Afghanistan. Slip in the 1892 earthquake extended for at least 60 km according to *Lawrence et al.* [1992], which is consistent with M6.5, mean slip of 0.8 m, and a locking depth of 4 km. *Griesbach* [1893] indicates that surface rupture from this earthquake extended southward from the point where the railroad crosses the fault (30.85°N 66.52°E) for some distance, but did not extend much farther to the north. Our GPS transect across the Chaman Fault lies 2 km north of this railroad crossing possibly sampling a northward transition in locking depth analogous to that observed south of Parkfield on the San Andreas fault [*Lienkaemper et al.*, 2006]. Indeed, the occurrence of serpentinite on the fault at this location may also provide a lithological and rheological justification for this transition [*Lawrence and Yeats*, 1979].

[47] Using cumulative seismic moment estimates, previous authors have noted a slip deficit on the Chaman fault system north of ~31°N [*Bernard et al.*, 2000; *Ambraseys and Bilham*, 2003b]. Given the observed interseismic deformation rates of 16.8 ± 2.7 mm/yr near Qalat, Afghanistan and 16.8 ± 0.51 near Kabul, Afghanistan, one would expect M_w 7.0 earthquakes every 60–90 years; this is not the case, and as it is likely that the seismic catalog of this region is complete above M 6.5 since at least 1890 [*Ambraseys and Bilham*, 2003a], the absence of earthquakes with magnitudes $M > 7$ in the historical record suggests that the region of the Chaman Fault near Qalat may have accumulated enough strain for a large earthquake. Further, this observation suggests that the low Peak Ground Acceleration prediction for this region for the next 50 years presented by the *Pakistan Meteorological Department* [2007] may be too conservative. However, our observed locking depths and the measured slip rate are consistent with the absence of $M_w > 7$ earthquakes in the historical record, and the observed productivity of $5 < M_w < 5.5$ earthquakes on the central Chaman fault. Earthquakes of M_w 5.5 with a locking depth of 5 km, a rupture length of 5 km, and coseismic slip of 30 cm would be associated with renewal times of ~20 years. While surface creep along the Chaman Fault has been suggested as an explanation for this moment deficit, our data do not favor surface creep north of Chaman (Figure 11).

[48] The active plate boundary is offset more than 20 km to the west of the mapped Ornach Nal fault near Bela. Although the GPS station density is too low to provide an accurate constraint on the locking depth of the plate boundary ($2.9^{+9.1}_{+0}$ km) in the Ornach-Nal region, the low seismic productivity combined with the high interseismic deformation rate shown by the GPS transect ($15.1^{+16.9}_{+13.4}$ mm/yr) suggests that the locking depth along the plate boundary is either shallow or accommodated across multiple structures. No through going surface fault exists at the location of maximum geodetic shear although we have identified a number of weak morphological lineations using Landsat imagery (Figure 7) that may be associated with incipient subsurface shear. The formation of a prominent basin, the Hinglaj synform, is consistent with a pull apart between two left-stepping sinistral shears.

[49] An alternative interpretation — that the active plate boundary dips to the west and is creeping at depth below the region of maximum shear, emerging at the surface near the mapped Ornach Nal fault — is considered less likely for two reasons. The first argument is that previous authors have supposed the thick package of mud that forms the mountains to the west of Bela to represent an intruded inhomogeneous lubricant similar to the mud volcanoes found elsewhere in the region. In fact the muds consist of a steeply dipping sedimentary series in stratigraphic sequence and with little internal deformation, which may in part be the source of eruptive material from nearby mud volcanoes [*Delisle*, 2005, 2004; *Delisle et al.*, 2002]. The second argument is that the weakly constrained locking depth of $2.9^{+9.1}_{+0}$ km would require the fault to dip at a shallow angle between 13–36°W were it to emerge at the foot of the range where the Ornach Nal fault is mapped. It is difficult to conceive of an efficient continental transform with this geometry.

[50] Historically, the Ornach-Nal region has been seismically quiet [*Zaigham*, 1991; *Lawrence et al.*, 1992]; even *Minchin* [1907], in his "Gazateer of Las Bela", notes that this region is not prone to earthquakes. Since the 1950's, the ISC catalog has bolstered this view, listing no seismicity near the Ornach-Nal Fault before 1972 (Figure 2a). During the 1970's the increasing density of the global seismic network led to an increase in sensitivity to small magnitude earthquakes, yet the ISC lists no earthquakes larger than M_b 4.9 near the Ornach-Nal Fault during the period 1972–2010. The low magnitude of these earthquakes combined with sparse regional seismic network coverage results in very poor depth constraints in this area. Although the GPS station density is too low to provide an accurate constraint on the locking depth of the plate boundary in the Ornach-Nal region, the low seismic productivity combined with the high interseismic deformation rate shown by the GPS transect ($15.1^{+16.9}_{+13.4}$ mm/yr) suggests that the locking depth along the plate boundary is shallow.

[51] Modeling of Bouger gravity transects between Karachi and the Ornach-Nal Fault by *Zaigham* [1991] suggests the presence of east-dipping subducted oceanic crust beneath the southern Kirthar Range. Although depth estimates for earthquakes in the Ornach-Nal region are poor, the presence of sparse, deep seismicity combined with the interpretation of an east-dipping crustal layer prompted *Zaigham* [1991] to suggest on-going subduction of this crustal sliver, which he termed the Makran-Bela microplate. However, the low eastward convergence velocity of stations LAKC and SHFD west of Bela and the southern Kirthar Range (~2 mm/yr) suggests that subduction of this sliver has ceased.

[52] In Figure 13, we compare the measurements and the maximum sinistral and fault-normal deformation estimates made from pole-of-rotation parameters published in *Altamimi et al.* [2011a]. Estimates along each fault shown in Figure 13 assume that slip is perfectly partitioned across each fault. Since all four estimates of sinistral motion and

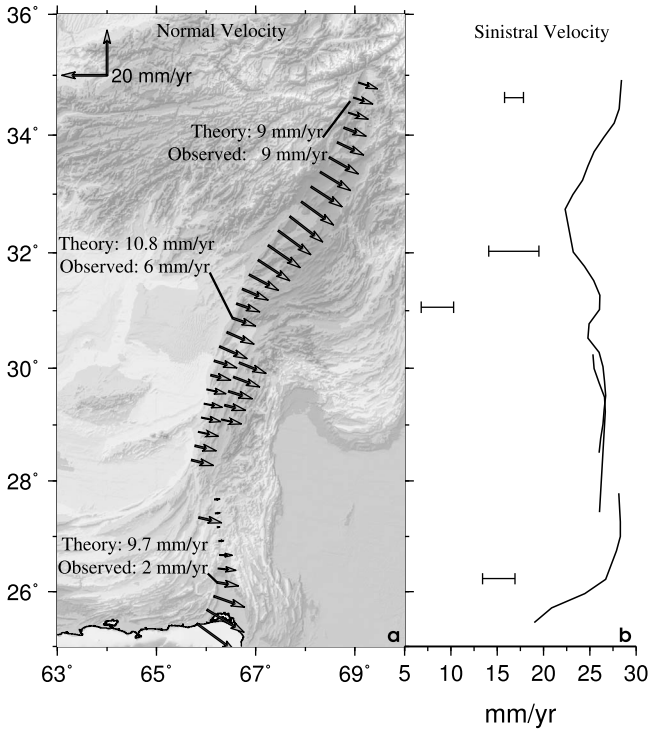

Figure 13. Maximum fault-normal and fault-parallel velocities based on ITRF2008 pole-of-rotation locations and rates published in *Altamimi et al.* [2011a] projected along mapped faults on the western boundary of the India Plate. Estimates are derived using the azimuth of the surface trace of plate bounding faults and assume that slip partitioning is perfect and occurs only along a single fault. (a) Maximum convergence estimated assuming perfect partitioning of slip. Locations of convergence observations indicated by text. (b) Maximum sinistral motion estimated assuming perfect partitioning of slip. Locations of sinistral motion estimates indicated by horizontal bars and represent 95% confidence intervals. Note all three measurements of sinistral motion and both measurements of fault-normal motion suggest lower rates compared with perfect slip partitioning.

two of the estimates of convergence are lower than the expected velocities calculated under the assumption of perfect slip partitioning, this suggests that both sinistral slip and convergence are likely accommodated across multiple structures. In the south, across the Ornach-Nal Fault, the faults across the Hinglaj Synform appear to accommodate the majority of the sinistral plate motion. Similarly, in the north, across the Chaman Fault near Qalat, Afghanistan, the Chaman Fault appears to accommodate the majority of the sinistral plate motion. At the latitude of Chaman, Pakistan, however, the large deficit in sinistral deformation suggests that most of the sinistral plate motion is accommodated by faults to the east. At the latitude of Kabul, Afghanistan, the baseline between GPS stations NCEG and KBUL only samples the deformation across one of the major sinistral faults in the Chaman fault system, the Gardez fault. Thus, given the relatively low seismicity rates farther west of Kabul (Figure 2) [*Ambraseys and Bilham* [2003a], the remaining 11.4 mm/yr are likely accommodated across the Chaman fault proper, just west of our transect. The agreement between ITRF2008 and observation in convergence rate across this same transect is supplemented by the occurrence of thrust faulting earthquakes in the region with NE striking nodal planes (Figure 2). However, the lack of geological mapping in this region makes further interpretation difficult. We also note that the upper limits of observed strike-slip (∼17 mm/yr) are similar to convergence rates reported in the western Himalaya [*Apel et al.*, 2006; *Bendick et al.*, 2007; *Mohadjer et al.*, 2010].

7. Conclusions

[53] We present interseismic deformation rates and locking depth estimates for three locations across the Chaman Fault System using space geodetic techniques. Along the southern Chaman Fault System, the Ornach-Nal fault represents the obvious plate bounding fault. Near the town of Bela, geodetic measurements across the fault indicate that the plate boundary is actually located $12.5^{+35}_{+5.6}$ km west of the Ornach-Nal Fault beneath the Hinglaj Synform. Assuming deformation is accommodated across a single fault strand, strain is accumulating at a rate of $15.1^{+16.9}_{+13.4}$ mm/yr and is locked to a depth of $2.9^{+9.1}_{+0}$ km. The absence of historical and modern seismicity, and the low relative velocities of Bela, Pakistan relative to the India Plate suggests that aseismic deformation may accommodate an additional ≈10 mm/yr west of the plate boundary, most probably on the Ghazaband fault. Farther north, at the latitude of Chaman, Pakistan, the Chaman Fault appears to accommodate as little as 40% of the overall sinistral motion across the plate boundary with the remaining deformation distributed across faults between the Chaman fault and the Seistan Ranges. Geodetic data suggest that the fault is very shallowly locked ($3.4^{+7.0}_{+0}$ km) and accumulating strain at a rate of $8.5^{+10.3}_{+6.8}$ mm/yr. Although we observe no significant strain accumulation across the extreme northernmost segment of the Ghazaband Fault, it is likely that this fault accommodates a large portion of the sinistral motion of the plate boundary at latitudes south of Quetta, Pakistan. North of the town of Chaman, Pakistan, interseismic deformation across the Chaman fault is consistent with 16.8 ± 2.7 mm/yr of slip beneath a 5.4 ± 2.4 km thick locked elastic lid near Qalat, Afghanistan and 16.8 ± 0.51 mm/yr near Kabul, Afghanistan. Since there have been no recorded earthquakes with $M_w > 6.5$ on these segments of the fault system in the past 115 years, it is possible that these segments rupture in earthquakes with magnitudes larger than M_w 7 with return intervals of >120 years.

[54] **Acknowledgments.** We thank Chuck Lindsay of the U.S. Geological Survey, Denver, who was responsible for the important initial installation of the Kabul GPS measurement point, and Solmaz Mohadjer at the Aga Khan Development Network, Disaster Risk Management Initiative for its subsequent remeasurement. This research was supported by the National Science Foundation under grant EAR-0229690. Support for GPS fieldwork in Baluchistan was also provided by the Pakistan Science Foundation. ERS and Envisat data were provided by the European Space Agency under category-1 proposal 2757 and were processed using the JPL/Caltech software package ROI_PAC [*Rosen et al.*, 2004]. Original InSAR data are copyright of the European Space Agency. Occupation and maintenance of continuous and campaign Global Positioning System (GPS) receivers was performed by Din Mohammad Kakar of the University of Baluchistan, Quetta, Pakistan and Sarosh Lodi of the NED University, Karachi, Pakistan. GPS data were processed using the MIT GAMIT/

GLOBK software package [*Herring et al.*, 2010a, 2010b]. International Seismological Centre (ISC) and Engdahl, van der Hilst, and Buland (EHB) catalog data were retrieved from http://www.isc.ac.uk. Landsat imagery was acquired using the U.S. Geological Survey's Earth Explorer (http://edcsns17.cr.usgs.gov/EarthExplorer). All figures were created using Generic Mapping Tools [*Wessel and Smith*, 1998]. We would also like to thank Eric Fielding of the Jet Proplusion Laboratory, Gareth Funning of the University of California, Riverside, Rowena Lohman of Cornell University, and Tim Wright of the University of Leeds for discussion on InSAR processing techniques. Gareth Funning provided software for InSAR inversion, and Rowena Lohman provided software for InSAR data resampling.

References

Altamimi, Z., L. Métivier, and X. Collilieux (2011a), ITRF2008 plate motion model, *Geophys. Res. Abstr.*, *13*, EGU2011-4750.

Altamimi, Z., X. Collilieux, and Métivier (2011b), ITRF2008: An improved solution of the international terrestrial reference frame, *J. Geod.*, *85*, 457–473, doi:10.1007/s00190-011-0444-4.

Ambraseys, N., and R. Bilham (2003a), Earthquakes in Afghanistan, *Seismol. Res. Lett.*, *74*(2), 107–123.

Ambraseys, N., and R. Bilham (2003b), Earthquakes and associated deformation in northern Baluchistan, *Bull. Seismol. Soc. Am.*, *93*(4), 1573–1605.

Ambraseys, N., and J. J. Douglas (2004), Magnitude calibration of north Indian earthquakes, *Geophys. J. Int.*, *159*, 165–206.

Ambraseys, N., and D. Jackson (2003), A note on early earthquakes in northern India and southern Tibet, *Curr. Sci. India*, *84*(4), 570–582.

Apel, E., R. Burgmann, P. Bannerjee, and B. Nagarajan (2006), Geodetically constrained Indian Plate motion and implications for plate boundary deformation, *Eos Trans. AGU*, *85*(52), Fall Meet. Suppl., Abstract T51B-1524.

Babur, Z. M. (1912), *The Babur-nama in English*, translated by A. S. Beveredge, Steven Austin, Hertford, U. K.

Baird Smith, R. (1843), Memoir of Indian earthquakes—Part II, *J. Asiat. Soc. Bengal*, *12*(144), 1029–1056.

Bannert, D., A. Cheema, A. Ahmed, and U. Schaffer (1992), The structural development of the Western Fold Belt, Pakistan, *Geol. Jahrb.*, *80*, 3–60.

Bendick, R., R. Bilham, M. A. Khan, and S. F. Khan (2007), Slip on an active wedge thrust from geodetic observations of the 8 October 2005 Kashmir earthquake, *Geology*, *35*(3), 267–270.

Berardino, P., R. Lanari, and E. Sansosti (2002), A new algorithm for surface deformation monitoring based on small baseline differential SAR interferograms, *IEEE Trans. Geosci. Remote Sens.*, *40*(11), 2375–2383.

Bernard, M., B. Shen-Tu, W. E. Holt, and D. M. Davis (2000), Kinematics of active deformation in the Sulaiman lobe and range, Pakistan, *J. Geophys. Res.*, *105*(6), 13,253–13,279.

Beun, N., P. Bordet, and J.-P. Carbonnel (1979), Premières données quantitatives relatives au coulissage du décrochement de Chaman (Afghanistan du Sud-Est), *C. R. Acad. Sci. Paris*, *288*, 931–934.

Biggs, J., T. J. Wright, L. Zhong, and B. Parsons (2007), Multi-interferogram method for measuring interseismic deformation: Denali fault, Alaska, *Geophys. J. Int.*, *170*, 1165–1179.

Bürgmann, R., P. A. Rosen, and E. Fielding (2000), Synthetic aperature radar interferometry to measure Earth's surface topography and its deformation, *Annu. Rev. Earth Planet. Sci.*, *28*, 169–209.

Cox, P., N. Cater, and W. Goodenough (1936), The Quetta earthquake: Discussion, *Geogr. J.*, *88*(5), 428–430.

Delisle, G. (2004), Mud volcanoes of Pakistan, *Environ. Geol.*, *46*, 1024–1029.

Delisle, G. (2005), Mud volcanoes of Pakistan—An overview, in *Mud Volcanoes, Geodynamics and Seismicity*, edited by G. Martinelli and B. Panahi, pp. 159–169, Springer, Dordrecht, Netherlands.

Delisle, G., U. von Rad, H. Andruleit, C. H. von Daniels, A. B. Tabrez, and A. Inam (2002), Active mud volcanoes on- and offshore eastern Makran, Pakistan, *Int. J. Earth Sci.*, *91*, 93–110.

Engdahl, E. R., and A. Villasenor (2002), Global seismicity: 1900–1999, in *International Handbook of Earthquake and Engineering Seismology*, vol. A, edited by W. H. K. Lee et al., chap. 41, pp. 665–690, Academic, Amsterdam.

Farr, T. G., et al. (2007), The shuttle radar topography mission, *Rev. Geophys.*, *45*, RG2004, doi:10.1029/2005RG000183.

Goldstein, R. M., and C. L. Werner (1998), Radar interferogram filtering for geophysical applications, *Geophys. Res. Lett.*, *25*(21), 4035–4038.

Goldstein, R. M., H. A. Zebker, and C. L. Werner (1988), Satellite radar interferometry: Two-dimensional phase unwrapping, *Radio Sci.*, *23*(4), 713–720.

Griesbach, C. L. (1893), Notes on the earthquake in Baluchistan on the 20th December 1892, *Rec. Geol. Surv. India*, *26*(2), 57–61.

Hanssen, R. F. (2001), *Radar Interferometry: Data Interpretation and Error Analysis*, *Remote Sens. Digital Image Process.*, vol. 2, Kluwer Acad., Dordrecht, Netherlands.

Haq, S. S. B., and D. M. Davis (1997), Oblique convergence and the lobate mountain belts of western Pakistan, *Geology*, *25*(1), 23–26.

Herring, T. A. (2003), MATLAB tools for viewing GPS velocities and time series, *GPS Solut.*, *7*, 194–199, doi:10.1007/s10291-003-0068-0.

Herring, T. A., R. W. King, and S. C. McClusky (2010a), GAMIT reference manual, GPS analysis at MIT release 10.4, report, 171 pp., Dep. of Earth Atmos. and Planet. Sci., Mass. Inst. of Technol., Cambridge.

Herring, T. A., R. W. King, and S. C. McClusky (2010b), GLOBK: Global Kalman filter VLBI and GPS analysis program, release 10.4, report, 95 pp., Dep. of Earth Atmos. and Planet. Sci., Mass. Inst. of Technol., Cambridge.

Hooper, A. (2008), A multi-temporal InSAR method incorporating both persistent scatterer and small baseline approaches, *Geophys. Res. Lett.*, *35*, L16302, doi:10.1029/2008GL034654.

Jones, A. (Ed.) (1961), *Reconnaissance Geology of Part of West Pakistan: A Columbo Plan Cooperative Project*, Gov. of Pakistan, Oshawa.

Landor, A. H. S. (1902), *Across Coveted Lands or a Journey From Flushing (Holland) to Calcutta Overland*, Macmillan, London.

Lawrence, R. D., and R. S. Yeats (1979), Geological reconnaissance of the Chaman Fault in Pakistan, in *Geodynamics of Pakistan*, edited by A. Farah and K. A. DeJong, pp. 351–357, Geol. Surv. of Pakistan, Quetta.

Lawrence, R. D., S. H. Khan, and T. Nakata (1992), Chaman Fault, Pakistan-Afghanistan, *Ann. Tecton.*, *6*, 196–223.

Lienkaemper, J. J., B. Baker, and F. S. McFarland (2006), Surface slip associated with the 2004 Parkfield, California, earthquake measured with alinement arrays, *Bull. Seismol. Soc. Am.*, *96*(4), 239–249.

Massonnet, D., and K. Feigl (1995), Discrimination of geophysical phenomena in satellite radar interferograms, *Geophys. Res. Lett.*, *22*(12), 1537–1540.

Minchin, C. F. (Ed.) (1907), *The Gazatteer of Las Béla*, *District Gazatteer Ser. of Baluchistán*, vol. 8, Times Press, Bombay, India.

Mohadjer, S., et al. (2010), Partitioning of India-Eurasia convergence in the Pamir-Hindu Kush from GPS measurements, *Geophys. Res. Lett.*, *37*, L04305, doi:10.1029/2009GL041737.

Mosegaard, K., and A. Tarantola (1995), Monte Carlo sampling of solutions to inverse problems, *J. Geophys. Res.*, *100*(7), 12,431–12,447.

Oldham, T. (1883), A catalogue of Indian earthquakes from the earliest time to the end of A.D. 1869, *Mem. Geol. Surv. India*, *29*, 163–215.

Pakistan Meteorological Department (2007), Seismic hazard analysis and zonation for Pakistan, Azad Jammu and Kashmir, report, 156 pp., Pakistan Meteorol. Dep., Islamabad.

Parsons, B., et al. (2006), The 1994 Sefidabeh (eastern Iran) earthquake revisited: New evidence from satellite radar interferometry and carbonate dating about the growth of an active fold above a blind thrust fault, *Geophys. J. Int.*, *164*, 202–217.

Pinhey, L. A. (1938), The Quetta earthquake of 31 May 1935, report, 26 pp., Govt. of India Press, New Delhi.

Ramanathan, K. R., and S. M. Mukherji (1938), A seismological study of the Baluchistan (Quetta) earthquake of May 31, 1935, *Rec. Geol. Surv. India*, *73*(4), 483–513.

Reilinger, R., et al. (2006), GPS constraints on continental deformation in the Africa-Arabia-Eurasia continental collision zone and implications for the dynamics of plate interactions, *J. Geophys. Res.*, *111*, B05411, doi:10.1029/2005JB004051.

Rosen, P. A., S. Hensley, G. Peltzer, and M. Simons (2004), Updated Repeat Orbit Interferometry package released, *Eos Trans. AGU*, *85*(5), 35.

Savage, J. C., and R. O. Burford (1973), Geodetic determination of relative plate motion in central California, *J. Geophys. Res.*, *78*(5), 832–845.

Segall, P., and J. L. Davis (1997), GPS applications for geodynamics and earthquake studies, *Annu. Rev. Earth Planet. Sci.*, *25*, 301–336.

Skrine, C. P. (1936), The Quetta earthquake, *Geogr. J.*, *88*(5), 414–428.

Snead, R. E. (1964), Active mud volcanoes of Baluchistan, west Pakistan, *Geogr. Rev.*, *54*(4), 546–560.

Szeliga, W., R. Bilham, D. Schelling, D. M. Kakar, and S. Lodi (2009), Fold and thrust partitioning in a contracting fold belt: Insights from the 1931 Mach earthquake in Baluchistan, *Tectonics*, *28*, TC5019, doi:10.1029/2008TC002265.

Szeliga, W., S. E. Hough, S. Martin, and R. Bilham (2010), Intensity, magnitude, location and attenuation in India for felt earthquakes since 1762, *Bull. Seismol. Soc. Am.*, *100*(2), 570–584.

Wellman, H. W. (1966), Active wrench faults of Iran, Afghanistan and Pakistan, *Geol. Rundsch.*, *55*(3), 716–735.

Wells, D. L., and K. J. Coppersmith (1994), New empirical relationships among magnitude, rupture length, rupture width, rupture area, and surface displacement, *Bull. Seismol. Soc. Am.*, *84*(4), 974–1002.

Wessel, P., and W. H. F. Smith (1998), New improved version of Generic Mapping Tools released, *Eos Trans. AGU*, *79*, 579.
Williams, S. (2008), CATS: GPS coordinate time series analysis software, *GPS Solut.*, *12*, 147–153, doi:10.1007/s10291-007-0086-4.
Wright, T. J., B. Parsons, and E. Fielding (2001), Measurement of interseismic strain accumulation across the North Anatolian Fault by satellite radar interferomety, *Geophys. Res. Lett.*, *28*(10), 2117–2120.
Yeats, R. S., R. D. Lawrence, S. Jamil-ud din, and S. H. Khan (1979), Surface effects of the 16 March 1978 earthquake, Pakistan-Afghanistan border, in *Geodynamics of Pakistan*, edited by A. Farah and K. A. DeJong, pp. 159–361, Geol. Surv. of Pakistan, Quetta.
Zaigham, N. A. (1991), Bela ophiolites and associated mineralization in southern part of axial-belt of Pakistan, PhD thesis, Univ. of Karachi, Karachi, Pakistan.